



ELSEVIER

Contents lists available at ScienceDirect

Journal of Luminescence

journal homepage: www.elsevier.com/locate/jlumin

Full Length Article

Visible–NIR emission and structural properties of Sm^{3+} doped heavy-metal oxide glass with composition $\text{B}_2\text{O}_3\text{–PbO–Bi}_2\text{O}_3\text{–GeO}_2$

A. Herrera^{a,b}, R.G. Fernandes^c, A.S.S. de Camargo^c, A.C. Hernandez^c, S. Buchner^d,
C. Jacinto^b, N.M. Balzaretto^{a,*}

^a Instituto de Física, Universidade Federal do Rio Grande do Sul, Av. Bento Gonçalves 9500 - Caixa Postal 15051, CEP 91501-970 Porto Alegre, RS, Brazil

^b Grupo de Fotônica e Fluidos Complexos, Instituto de Física, Universidade Federal de Alagoas, 57072-900 Maceió, AL, Brazil

^c Instituto de Física de São Carlos, Universidade de São Paulo, Av. Trabalhador São-carlense, 400, CEP 13566-590 São Carlos, SP, Brazil

^d Universidade Federal de Ciências da Saúde de Porto Alegre, Rua Sarmento Leite, 245, CEP 90050-170 Porto Alegre, RS, Brazil

ARTICLE INFO

Article history:

Received 23 June 2015

Accepted 27 October 2015

Available online 17 November 2015

Keywords:

Heavy metal oxide glasses

Samarium

Judd Ofelt theory

Photoluminescence

ABSTRACT

A highly transparent Sm^{3+} glass with composition $\text{B}_2\text{O}_3\text{–PbO–Bi}_2\text{O}_3\text{–GeO}_2$ was obtained by the traditional melt quenching technique and characterized from structural and spectroscopic points of view. Analysis by X-ray diffraction and Raman spectroscopy confirmed the amorphous nature of the sample and revealed the expected low phonon energy. Differential thermal analysis was also carried out to obtain the glass transition and the crystallization temperatures, related to the thermal stability of the sample. Judd–Ofelt theory was applied to evaluate phenomenological intensity parameters Ω_λ ($\lambda=2, 4$ and 6) from the optical absorption measurements. The transition probabilities, radiative lifetimes, branching ratio and stimulated emission cross-section were also calculated. Photoluminescence spectra recorded in the visible and infrared regions revealed intense green, orange, red and near infrared emission bands providing a new trace to develop tunable laser and optoelectronics devices.

© 2015 Elsevier B.V. All rights reserved.

1. Introduction

Crystals and glasses doped with trivalent rare-earth (RE) ions have been largely investigated for more than 30 years for photonic applications such as in optical fibers, fluorescent devices, detectors and optical waveguides [1–3]. The spectral properties of these ions depend, to some extent, on the chemical and structural composition of the glassy or crystalline host matrix [4]. Many compositions have been studied in the search for more efficient ion–host combinations that will ultimately lead to reduced suppression of luminescence [2]. Despite their usually high phonon energies that can negatively affect the quantum yield of RE ions, oxide glasses exhibit fairly high transmission window, good thermal, chemical and mechanical stability and large RE incorporation [5,6]. In order to overcome the drawback of high frequency vibrations, heavy metal oxide glasses (HMOG), especially those containing Bi_2O_3 and PbO , have been investigated [6]. Among different possibilities, the choice of the network former B_2O_3 ensures a wide glass-forming range allowing the incorporation of modifier constituents such as GeO_2 and Bi_2O_3 to tailor specific properties. Besides the usual suitable features of oxide glasses, such compositions present high density and high

linear and nonlinear refractive indexes, broad transmission window and low phonon energy enabling applications in several optoelectronic devices [7].

The optical spectra of RE ions in glasses provide important information about the effect of host–ion interaction on the electronic and vibrational energy levels of the material, which are essential for the design of applications [8]. Beyond the experimental approach, a theoretical treatment using the Judd–Ofelt (JO) formalism [9,10] allows the determination of the spectral intensities of RE's electronic transitions.

The optical properties of Sm^{3+} ions have been reported for a large number of glassy systems [11–13] with a typical concentration of 1.0 mol% of Sm^{3+} . Compared to other RE ions, Sm^{3+} stands out due to its optical luminescence in the visible region (VIS), however, little attention has been paid to emissions in the near infrared (NIR) region [14]. It is a four-level laser system similar to Nd^{3+} , favoring laser emission, and it allows, also, thermal sensing applications [15]. Farries et al. [16] reported a Sm^{3+} -doped silica optical fiber laser operating at 651 nm using a 488 nm argon ion laser as a pumping source and Zhang et al. [17] investigated the luminescence properties of Sm^{3+} doped phosphor for white light emitting diodes. However, severe aggregation of Sm^{3+} at high doping concentration levels has been reported for some glasses [18]. Sm^{3+} ions also present valence instability and, for some glasses, negative values are obtained for the JO phenomenological

* Corresponding author. Tel.: +55 51 3308 6489.

E-mail address: naira@if.ufrgs.br (N.M. Balzaretto).

intensity parameters [19–21]. JO theory is applicable when the high f-splitting is small compared to the f-d energy gap and, therefore, it is inappropriate for calculating the Ω_λ for Sm^{3+} . Nonetheless, the JO theory has been used to investigate Sm^{3+} doped glasses for applications such as in photodynamic therapy (PDT) [22], solar cells substrates [23], laser emission [16] and white light diodes [17], among others.

In this work the structural and spectroscopic characteristics of a new lead-containing borate glass with composition $\text{B}_2\text{O}_3\text{-PbO-GeO}_2\text{-Bi}_2\text{O}_3\text{-Sm}_2\text{O}_3$ (BPGb:Sm) were investigated, revealing efficient visible (VIS) and novel near infrared (NIR) emissions. The probabilities of spontaneous emission and the maximum stimulated emission cross-sections were calculated using the JO theory.

2. Experimental

A glass with composition 26.66 $\text{B}_2\text{O}_3\text{-52.33PbO-16GeO}_2\text{-4Bi}_2\text{O}_3\text{-1Sm}_2\text{O}_3$ (BPGb:Sm) was prepared by the traditional melt quenching technique. The starting materials B_2O_3 , PbO and Bi_2O_3 (Alfa-Aesar, 99.99%), GeO_2 (Preussaug Mettal-Goslar) and Sm_2O_3 (Aldrich, 99.99%) were thoroughly mixed in a 30 g batch and heated at 850 °C for 15 min in Pt crucible in air. The melt was poured onto a graphite mold preheated at 270 °C to avoid thermal shock, and annealed at 50 °C for 12 h, below the glass transition temperature (383 °C), to release mechanical stress. Finally, the glass was slowly cooled down to room temperature and cut and polished for optical measurements. The amorphous nature of the sample was confirmed by X-ray powder diffraction using a diffractometer Siemens model D500. The thermal stability against crystallization was verified by DTA (Differential Thermal Analysis) using a Shimadzu analyzer model DTA 50 in the temperature range 20–800 °C, at a rate of 10 °C/min under Ar atmosphere.

The refractive index components (n_D , n_F and n_C) were measured using a Sopra GES- 5E ellipsometer. The volume density was calculated through the Archimedes method using an analytical balance Shimadzu model AUW220D (0.1 mg/0.01 mg) and distilled water as the immersion liquid. The used equation was as follows: $\rho_g = \rho_a w_g / (w_g - w_a)$, where ρ_g and ρ_a are the densities for sample and for water, respectively, w_g is the weight of the sample and w_a is the apparent immersed weight of the sample.

Room temperature absorption spectra in the UV–vis–NIR region were recorded using a high-performance spectrometer PerkinElmer model LAMBDA 1050 with a spectral resolution of 0.2 nm. Raman spectra were recorded in a Horiba Jobin Yvon iHR320 system using a 632.8 nm He–Ne excitation laser and a liquid nitrogen cooled CCD detector with a resolution of 0.5 cm^{-1} . Photoluminescence (PL) data were measured in a Crylas system using as excitation sources CW lasers at 266 nm and 488 nm. The PL signal was dispersed by an Acton SP2300 monochromator and detected by a Pixis 256E CCD. The luminescence intensity decay curve of the $^4\text{G}_{5/2}$ emitting level was measured using an electro-optic modulator to pulse the CW laser. The signal around 600 nm was dispersed by a SP2300 monochromator and detected by a Hamamatsu R955 photomultiplier. The detected signal was fed to a SR430 multichannel analyzer and transferred to a computer running acquisition software. The average lifetime value of the $^4\text{G}_{5/2}$ level was determined from a single exponential fit of the decay curve.

3. Theory

The quantitative analysis of the intensity of the absorption bands of trivalent lanthanides relates the experimentally determined oscillator strength f_{exp} to mechanisms by which radiation

can be absorbed. The experimental oscillator strength can be obtained from the expression $f_{\text{exp}} = \frac{mc}{\pi e^2 N} \int \alpha(\nu) d\nu$, where $\alpha(\nu)$ is the linear absorption coefficient as a function of the frequency ν (s^{-1}) and N is the concentration of rare earth ions. Following the conventional JO theory, the total theoretical oscillator strength f_{cal} of the induced electric dipole allowed transition $J \rightarrow J'$ is given by the following equation [9,10]:

$$f_{\text{cal}} = \frac{8\pi^2 mc \nu}{3h(2J+1)\chi} \sum_{\lambda=2,4,6} \Omega_\lambda (\psi J \| U^\lambda \| \psi' J')^2 \quad (1)$$

where the frequency ν corresponds to the transition from the ground state ψJ to the excited state $\psi' J'$, J and J' are the total angular momentum of the ground and excited states of the RE ion, respectively, $\chi = (n^2 + 2)^2 / 9n$ is the Lorentz local field correction for the refractivity of the medium, n is the linear refractive index, U^λ are the doubly reduced matrix elements of the unit tensor operator of rank $\lambda=2, 4, 6$, calculated from intermediate coupling approximation. The Ω_λ parameters are known as the JO phenomenological intensity parameters determined by a least-square fit of the theoretical and experimental oscillator strengths. The radiative lifetime τ_{rad} of an emitting state and the emission branching ratio $\beta_{JJ'}$ were calculated using conventional expressions: $\tau_{\text{rad}}(J) = \frac{1}{\sum_{J'} A_{\text{rad}}(JJ')}$ and $\beta_{JJ'} = \frac{A_{\text{rad}}(JJ')}{\sum_{J'} A_{\text{rad}}(JJ')}$, where A_{rad} is the radiative transition rate [24]. The branching ratio can be used to predict the relative intensities of all emissions lines originating from a given excited state.

4. Results and discussion

4.1. Structural and physical properties

The X-ray diffraction pattern of the BPGb:Sm glass shown in Fig. 1(a) confirmed its amorphous structure. Fig. 2(a) shows the DTA curve indicating the temperatures corresponding to the glass transition (T_g), softening (T_s), crystallization (T_x) and melting point (T_m). The slope in the range between 463 °C and 548 °C, after the glass transition temperature, is due to softening and sintering of the sample. The thermal stability parameter, defined as $\Delta T = T_x - T_g$, gives information about the resistance of the glass against crystallization, which is an important parameter for technological applications. For BPGb:Sm glass, $\Delta T \geq 170$ °C, making it a good candidate for optical devices [25–27]. For the undoped BPGb glass, $T_g = 333$ °C [6] while for BPGb:Sm, T_g increased to 383 °C, indicating a strong interaction between the Sm^{3+} ions and the host glass.

Fig. 1(c) presents the Raman spectrum for the BPGb:Sm glass. The low intensity band at $\sim 547 \text{ cm}^{-1}$ is related to the stretching of the symmetric Ge–O–Ge bonds [29] and the band at $\sim 759 \text{ cm}^{-1}$ is related to the symmetric Ge–O bonds [29,30]. The bands at ~ 913 and $\sim 1044 \text{ cm}^{-1}$ are assigned to ortho, penta and diborate groups [29–31]. The band at $\sim 1300 \text{ cm}^{-1}$ is related to BO_2O^- units connected to BO_4 units [6,29–31]. The spectra of doped and undoped samples look rather similar, giving no evidence of the structural influence of the doping ions. Another very important observation is that the most intense band is in the low energy range, specifically at 759 cm^{-1} , different from silicate systems that present intense vibrational bands around 1150 cm^{-1} [32].

From the measured values of density (ρ), refractive index n_D , concentration of Sm^{3+} ions ($N=1 \text{ mol}\%$) and average molecular weight, the polaron radius (r_p), mean inter-ionic distance (r_i), molar volume (V_m), molar refraction (R_m) and molar electronic polarizability (α_m) were calculated using standard equations [28]. These values along with the experimental thermal parameters are summarized in Table 1.

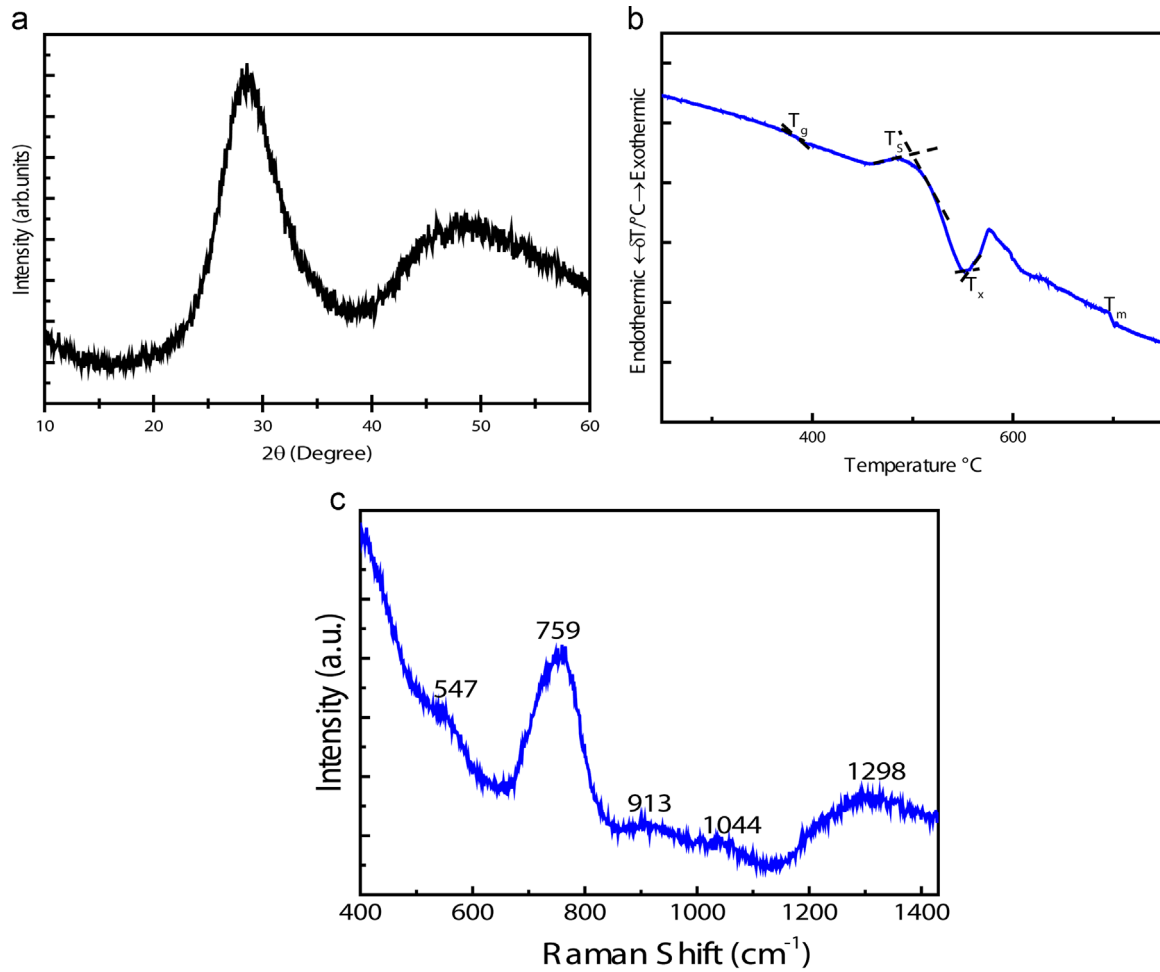


Fig. 1. (a) X-ray diffraction pattern, (b) differential thermal analysis and (c) Raman spectrum for BPGb:Sm glass sample.

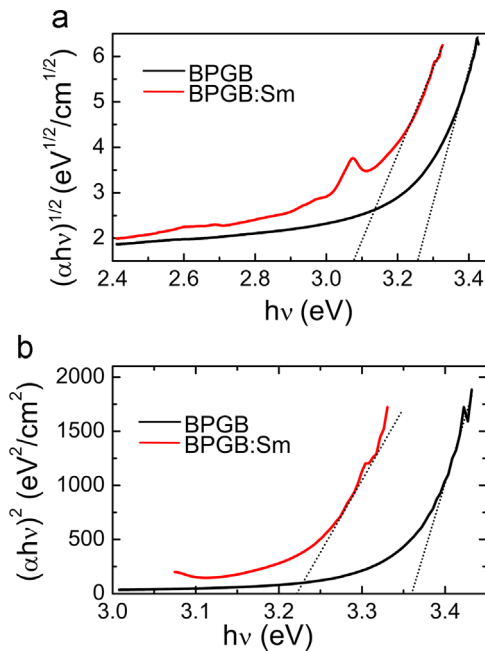


Fig. 2. (a) $(\alpha h\nu)^{1/2}$ and (b) $(\alpha h\nu)^2$ versus $h\nu$ for undoped (BPGb) and doped (BPGb:Sm) glasses.

Table 1

Measured and calculated physical properties for BPGb:Sm glass.

Density ρ (g/cm ³)	6.5
Refractive index	$n_D=1.9350$ $n_F=1.9440$ $n_C=1.9330$
T_g (°C)	383
T_x (°C)	556
T_s (°C)	498
$T_x - T_g$ (°C)	173
Abbe number	85
Concentration ($\times 10^{20}$ ions/cm ³)	2.25
Polaron radius r_p (Å)	6.6
Mean inter-ionic distance r_i (Å)	16.44
Molar volume V_m (cm ³ /mol)	26.43
Molar refraction R_m (cm ³ /mol)	12.77
Molar electronic polarizability α_m ($\times 10^{-24}$ cm ³)	5.066

4.2. Optical and spectroscopic properties

The linear absorption coefficient α near the UV absorption edge due to the host's electronic transitions, can be determined by [33]:

$$\alpha(\nu)h\nu = B(h\nu - E_g)^n \quad (2)$$

where B is a constant, $h\nu$ is the photon energy and E_g is the optical band gap. The parameter n is related to the electronic transition: $n=1/2$ for

allowed direct; $n=1/3$ for forbidden direct; $n=2$ for allowed indirect and $n=3$ for forbidden indirect transitions. Fig. 2(a) and (b) shows the Tauc's plots of $(\alpha h\nu)^{1/2}$ and $(\alpha h\nu)^2$ versus $h\nu$ for allowed indirect and direct transitions, respectively. The optical band gaps were obtained from the intercept of linear fits with the horizontal axis [34], giving 3.35 eV and 3.21 eV for allowed indirect transition and 3.26 eV and 3.07 eV for allowed direct transition in BPGB and BPGB:Sm glasses, respectively. The presence of Sm_2O_3 in small amounts in the glass composition may induce the formation of energy levels in the forbidden gap due to increase in the number of non-bridging oxygen species, changing the absorption spectrum [35].

The Urbach's plot, corresponding to $\ln(\alpha)$ versus $h\nu$, is shown in Fig. 3. Urbach's energy refers to the width of the tails of localized states in the forbidden zone of a disordered material. According to the rule of Urbach, the optical absorption coefficient curve near the absorption edge is an exponential function of the photon energy [34]. The values of ΔE were calculated taking the reciprocals of the slopes of the linear portion of the curves $\ln(\alpha)$ vs. $h\nu$, resulting in 0.28 eV and 0.30 eV for BPGB and BPGB:Sm glasses, respectively. The Urbach's energy increased with the introduction of Sm_2O_3 in the BPGB glass.

The absorption spectrum for the BPGB:Sm glass, presented in Fig. 4, shows seven absorption bands in the near infrared region, peaked at 750.8, 858.5, 977.9, 1095.0, 1178.8, 1219.2 and 1266.1 nm respectively, corresponding to absorption transitions from the ground state ${}^6\text{H}_{5/2}$ to the excited states ${}^6\text{F}_{11/2}$, ${}^6\text{F}_{9/2}$, ${}^6\text{F}_{7/2}$, ${}^6\text{F}_{5/2}$, ${}^6\text{F}_{3/2}$, ${}^6\text{H}_{15/2}$, ${}^6\text{F}_{1/2}$. Because the near-infrared transitions are spin allowed ($\Delta s=0$), they are rather intense.

The fluorescence spectra for Sm^{3+} doped BPGB:Sm glass in the VIS and NIR regions are presented in Fig. 5(a) and (b), respectively, revealing strong emissions in both regions. In the visible, the bands at 563, 601, 648, 711 and 786 nm correspond to the transitions from the excited state ${}^4\text{G}_{5/2}$ – ${}^6\text{H}_J$ ($J=5/2, 7/2, 9/2, 11/2, 13/2$)

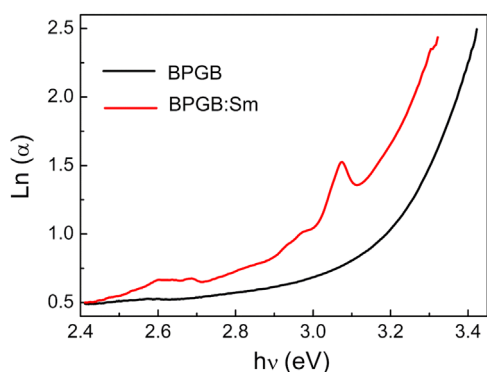


Fig. 3. $\ln(\alpha)$ versus $h\nu$ for undoped (BPGB) and doped (BPGB:Sm) glasses.

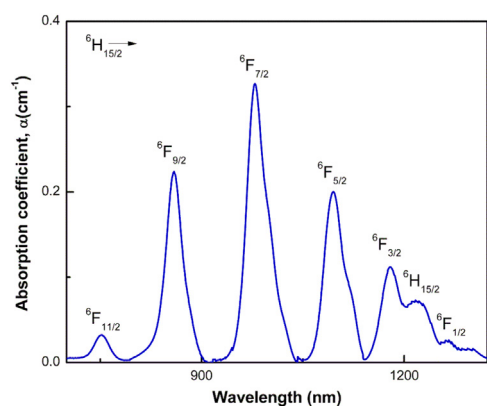


Fig. 4. Room temperature optical absorption spectrum of BPGB:Sm glass.

states of Sm^{3+} . The peaks in the NIR region centered at 912, 954, 1036 and 1182 nm correspond to transitions from the ${}^4\text{G}_{5/2}$ state to ${}^6\text{F}_J$ ($J=3/2, 5/2, 7/2, 9/2$). The energy level-diagram of the BPGB:Sm glass is presented in Fig. 6. It is important to note the large number of transitions observed, including the 1182 nm one, indicating that BPGB:Sm glass is a very efficient system.

Table 2 shows the experimental and calculated oscillator strengths with the corresponding root-means-square (δ_{rms}) values for the BPGB:Sm glass. The deviations are small, indicating a good fit, and the results for the JO parameters Ω_λ ($\lambda=2,4,6$) are consistent with previous results for other glasses doped with Sm [24,36].

Table 3 shows the values of Ω_λ ($\lambda=2, 4, 6$) calculated in the present work compared to values found in the literature for Sm^{3+} doped glasses. In general, the JO intensity parameters are host dependent and are useful indicators of the glass structure and transition rates of the rare earth ions [37]. The parameter Ω_2 rises drastically by lowering the symmetry of rare earth ligand field [38] and the covalence of the lanthanide ions [39]. In the present work, the value of the Ω_2 parameter is lower than those obtained for Sm^{3+} doped H_3BO_3 – Li_2CO_3 – CaCO_3 – PbO , ZnO – Sb_2O_3 – B_2O_3 , PbO – PbF_2 – B_2O_3 , PbO – PbF_2 glasses but higher than those obtained for Sm^{3+} doped telluride and PbO – H_3BO_3 – TiO_2 – AlF_3 – (LBTAf), as shown in the Table 3. A low value of Ω_2 suggests a symmetric environment around the Sm^{3+} ion site and a predominantly ionic bonding with the ligands. Nageno et al. [40] have studied alkali borate and phosphate glasses and concluded that Ω_4 and Ω_6 parameters depend on the viscosity and dielectric properties and are related to the rigidity of the glassy matrix. The ratio Ω_4/Ω_6 , known as spectroscopic quality factor [41], is important for predicting the stimulated emission for a laser medium. For BPGB:Sm, this ratio is 1.06, similar to values reported in the literature for other Sm^{3+} doped glasses [11,42–47], which suggests that it is a potential candidate for active laser medium.

Radiative transition probabilities A_{rad} (s^{-1}), branching ratio β_R and radiative lifetime τ_{rad} (ms) for BPGB:Sm glass are shown in Table 4. It is well-known that emission transitions with $\beta_R \geq 0.5$ are highly suitable for laser emission. The branching ratio value for the transition ${}^4\text{G}_{5/2}$ – ${}^6\text{H}_{7/2}$ for BPGB:Sm is 51.07%, which is similar to the values found for other Sm^{3+} doped glasses, as shown in Table 4, indicating the potential use of this transition for photonic applications.

The stimulated emission cross-section $\sigma(\lambda_p)(J,J')$ for transitions between J and J' has been used to identify the potential laser transitions of RE ions in any host material since a good laser transition should have large stimulated emission cross-section [47]. Table 5 presents the cross section values for the emission bands observed in this work, which are high compared to other Sm^{3+} doped glass matrices [42,48–50]. The highest value was observed for ${}^4\text{G}_{5/2}$ – ${}^6\text{H}_{7/2}$ transition ($6.08 \times 10^{-22} \text{ cm}^2$). The corresponding full-widths at half-maximum (FWHMs) for the novel NIR emission are 21.1, 26.0 and 31.7 nm, respectively. Despite the values of $\sigma(\lambda_p)(J,J')$ for NIR emissions being lower than those of VIS emissions, they are of the same order of magnitude. Therefore, the novel NIR emissions of BPGB:Sm provide a new clue for developing potential NIR optoelectronic devices [51].

The decay profile for BPGB:Sm glass is shown in Fig. 7. As can be observed in the inset, it is not a single exponential. A second order exponential fit was required and the average lifetime $\tau_{exp}=1.39$ ms was calculated [52], while the radiative lifetime obtained from the JO theory was $\tau_{rad}=2.58$ ms. The quantum efficiency η for the ${}^4\text{G}_{5/2}$ level, defined as $\eta = \frac{\tau_{exp}}{\tau_{rad}}$, was 54%, indicating that BPGB:Sm glass is a promising luminescent and laser material in the orange–red region [53].

The experimental lifetime can be expressed as $\frac{1}{\tau_{exp}} = \frac{1}{\tau_{rad} + w_{MPR} + w_{ET}}$, where w_{MPR} is the multiphonon relaxation that arises from the

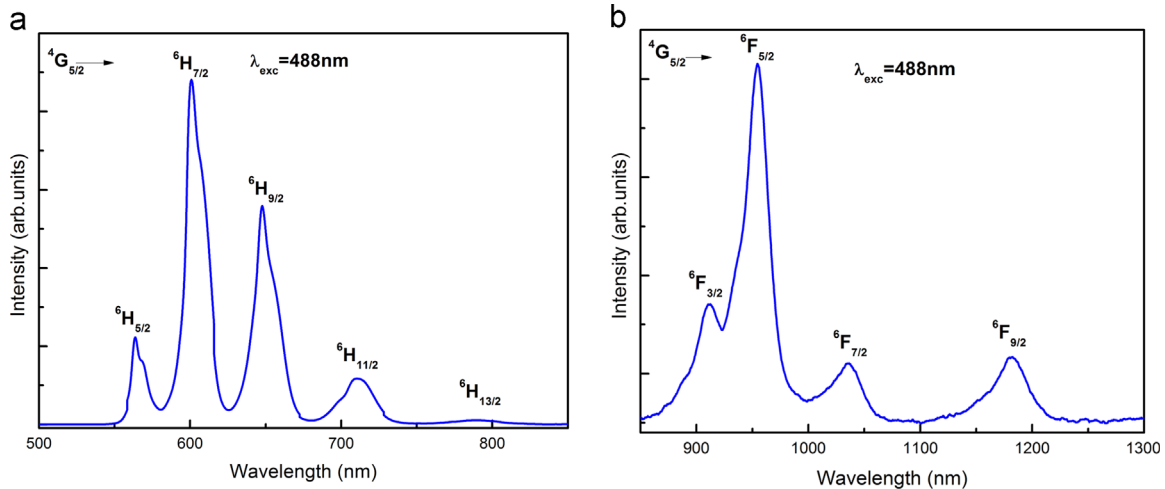


Fig. 5. (a) Visible and (b) near-infrared fluorescence spectra for BPGb:Sm glass under excitation at 488 nm.

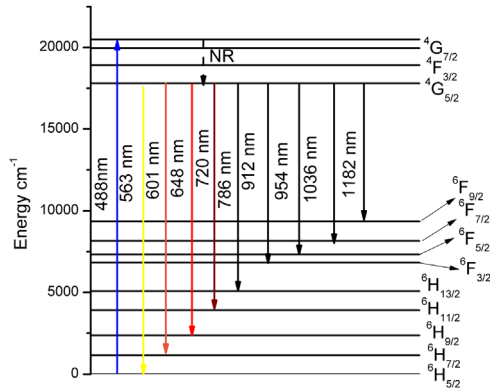


Fig. 6. Energy level diagram for BPGb:Sm glass.

Table 2

Experimental and calculated oscillator strengths for BPGb:Sm glass.

Transitions	Oscillator strength ($\times 10^{-6}$)	
	f_{exp}	f_{cal}
${}^6H_{5/2} \rightarrow {}^6F_{11/2}$	0.44	0.47
${}^6F_{9/2}$	2.66	2.83
${}^6F_{7/2}$	3.87	4.01
${}^6F_{5/2}$	2.00	1.90
${}^6F_{3/2} + {}^6H_{15/2} + {}^6F_{1/2}$	1.18	1.19
	$\delta_{rms} = 0.092 \times 10^{-6}$	

Table 3

Judd–Ofelt intensity parameters calculated for BPGb:Sm glass compared to values found in literature for other Sm^{3+} doped glasses.

Glass	Judd–Ofelt parameter (10^{-20} cm^2)			Trend	Ω_4/Ω_6
	Ω_2	Ω_4	Ω_6		
	Sm:Tellurite [42]	0.006	0.339		
Sm: LBTAf [11]	0.27	2.52	2.47	$\Omega_2 < \Omega_6 < \Omega_4$	1.02
Sm:BPGb (This work)	0.42	2.65	2.48	$\Omega_2 < \Omega_6 < \Omega_4$	1.06
$H_3BO_3-Li_2CO_3-CaCO_3-PbO$ [43]	0.97	5.04	4.73	$\Omega_2 < \Omega_6 < \Omega_4$	1.06
Sm:Lead fluoroborate [44]	3.41	2.92	2.17	$\Omega_6 < \Omega_4 < \Omega_2$	1.35
Sm:Silicate [45]	1.94	2.63	1.63	$\Omega_6 < \Omega_2 < \Omega_4$	1.62
Sm:PbO–PbF ₂ [46]	1.16	2.60	1.40	$\Omega_2 < \Omega_6 < \Omega_4$	1.86
Sm:Phosphate [47]	4.31	4.28	5.78	$\Omega_2 < \Omega_4 < \Omega_6$	0.74

Table 4

Radiative transition probabilities A_{rad} (s^{-1}), branching ratio β_R , and radiative lifetime τ_{rad} (ms) for the BPGb:Sm glass compared to the results found in the literature.

Transition from ${}^4G_{5/2}$ to	ΔE (cm^{-1})	BPGb:Sm		
		A_{rad}	β_R	τ_{rad}
${}^6H_{5/2}$	17701	35.83	0.0926	2.58
this work		20	0.1	
Sm: LBTAf [11]		2.117	0.023	
${}^6F_{9/2}$	16765.1	14.72	0.043	
Sm:Tellurite [42]		197.52	0.51	
Sm:Lead fluoroborate [44] (0.7 mol%)		102	0.50	
${}^6H_{7/2}$	16615	43.629	0.492	
this work		163.65	0.472	
Sm: LBTAf [11]		87.20	0.2254	
${}^6F_{7/2}$	15425	40	0.20	
Sm:Tellurite [42]		19.167	0.216	
Sm:Lead fluoroborate [44] (0.7 mol%)		106.82	0.308	
${}^6H_{9/2}$	15475.6	45.40	0.1174	
this work		23	0.11	
Sm: LBTAf [11]		11.829	0.133	
${}^6H_{11/2}$	14066	40.17	0.116	
Sm:Tellurite [42]		10482	14.28	0.0369
Sm:Lead fluoroborate [44] (0.7 mol%)		7	0.03	
${}^6F_{5/2}$	10523.1	1.331	0.015	
this work		10.74	0.031	
Sm:Tellurite [42]		9643	5.52	0.0143
${}^6F_{3/2}$	9652.8	3	0.01	
this work		1.038	0.011	
Sm:Tellurite [42]		3.28	0.009	
${}^6F_{1/2}$	8460	1.03	0.0027	
this work		0	0	
Sm: LBTAf [11]		8493.6	0.174	0.002
${}^6F_{3/2}$	8493.6	1.82	0.005	
Sm:Tellurite [42]				
Sm:Lead fluoroborate [44] (0.7 mol%)				

interaction between rare earth ions and the glass and w_{ET} is the energy transfer rate related to the ion–ion and ion–impurity interactions. For Sm^{3+} ions, w_{MPK} value is negligible due to the large energy gap of $\sim 7250 \text{ cm}^{-1}$ between the ${}^4G_{5/2}$ state and the next lower state ${}^6F_{11/2}$, requiring more than 8 phonons. The non-radiative contribution, w_{NR} , is due to the energy transfer among excited Sm^{3+} ions and possibly Sm^{3+} ions and residual impurities from the synthesis process. As a result, $w_{ET} = w_{NR} = \frac{1}{\tau_{rad} - \tau_{exp}} = 337 \text{ s}^{-1}$

Table 5

Stimulated emission cross-section $\sigma(\lambda_p)(J/J')$ for transitions from ${}^4G_{5/2}$ level in BPGb:Sm glass.

Transition ${}^4G_{5/2} \rightarrow$	λ_p (nm)	Δ_{eff} (nm)	$\sigma(\lambda_p)(J/J') (\times 10^{-22} \text{ cm}^2)$
${}^6H_{5/2}$	563	9.89	1.29
${}^6H_{7/2}$	601	15.03	6.08
${}^6H_{9/2}$	648	16.70	3.26
${}^6H_{11/2}$	711	23.40	1.75
${}^6F_{5/2}$	954	21.10	1.98
${}^6F_{7/2}$	1036	26.0	0.86
${}^6F_{9/2}$	1182	31.70	0.23

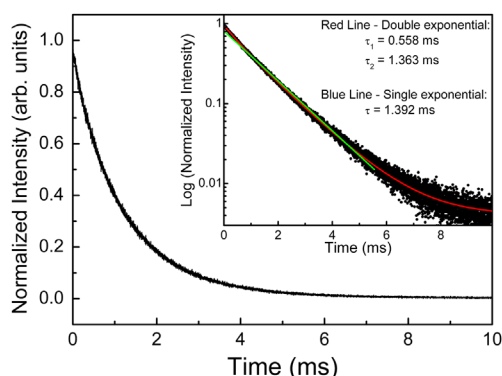


Fig. 7. Intensity decay profile for ${}^4G_{5/2}$ level in BPGb:Sm glass. Inset: Log of intensity decay versus time showing fits with single and double exponentials. (For interpretation of the references to color in this figure, the reader is referred to the web version of this article).

5. Conclusions

A Sm^{3+} -doped $\text{B}_2\text{O}_3\text{--PbO--Bi}_2\text{O}_3\text{--GeO}_2$ glass (BPGb:Sm) was obtained by conventional melt quenching technique. X-ray diffraction confirmed the amorphous nature. Differential thermal analysis (DTA) revealed that the BPGb:Sm glass is thermally stable. The Judd–Ofelt intensity parameters were calculated, as well as, the radiative transition rates, branching ratios, radiative lifetimes and stimulated emission cross-sections. Multichannel transition emissions were observed in the VIS and NIR regions. The quantum efficiency was determined to be 0.54. The obtained results indicated that BPGb:Sm glass should be suitable for laser and optoelectronic applications in the visible and near infrared regions.

Acknowledgments

Authors thank for the financial support of Brazilian agencies CAPES, CNPq and FAPERGS. They also thank for the Microelectronic Group (Paulo Franzen) for the spectroscopic characterization.

References

- [1] A.J. Kenyon, *Prog. Quantum Electron.* 26 (2002) 225.
- [2] M.J.F. Digonnet, Rare-earth-doped fiber lasers and amplifiers, 2001.
- [3] F. Auzel, *J. Alloy. Compd.* 275–277 (1998) 692.
- [4] G.C. Righini, M. Ferrari, *Riv. Del. Nuovo Cim.* 28 (2005) 1.
- [5] M. Mortier, A. Monteville, G. Patriarche, G. Maze, F. Auzel, *Opt. Mater. (Amst.)* 16 (2001) 255.
- [6] R.G. Fernandes, J. Ren, A.S.S. de Camargo, A.C. Hernandez, H. Eckert, *J. Phys. Chem. C* 116 (2012) 6434.

- [7] K. Terashima, T.H. Shimoto, T. Yoko, Structure and nonlinear optical properties of $\text{PbO--Bi}_2\text{O}_3\text{--B}_2\text{O}_3$ glasses, *Phys. Chem. Glas.* 38 (n.d) 211–217.
- [8] R. Reisfeld, *J. Less Common Metals* 93 (1983) 243.
- [9] B.R. Judd, *Phys. Rev.* 127 (1962) 750.
- [10] G.S. Ofelt, *J. Chem. Phys.* 37 (1962) 511.
- [11] B.C. Jamalajah, J. Suresh Kumar, A. Mohan Babu, T. Suhasini, L. Rama Moorthy, *J. Lumin.* 129 (2009) 363.
- [12] S. Shanmuga Sundari, K. Marimuthu, M. Sivraman, S.S. Babu, *J. Lumin.* 130 (2010) 1313.
- [13] K. Maheshvaran, K. Linganna, K. Marimuthu, *J. Lumin.* 131 (2011) 2746.
- [14] J. Yang, B. Zhai, X. Zhao, Z. Wang, H. Lin, *J. Phys. Chem. Solids* 74 (2013) 772.
- [15] U. Rocha, C. Jacinto Da Silva, W. Ferreira Silva, I. Guedes, A. Benayas, L. Martínez Maestro, et al., *ACS Nano* 7 (2013) 1188.
- [16] M.C. Farries, P.R. Morkel, J.E. Townsend, *Electron. Lett.* 24 (1988) 709.
- [17] J. Zhang, X. Wu, J. Zhu, Q. Ren, *Opt. Commun.* 332 (2014) 223.
- [18] M. Seshadri, K.V. Rao, J.L. Rao, Y.C. Ratnakaram, *J. Alloy. Compd.* 476 (2009) 263.
- [19] A.E. Sovestnov, V.A. Shaburov, G.A. Krutov Anomalous Behavior of $\text{Sm}^{2+}\text{--Sm}^{3+}$ Electronic Transition in solid solutions SmS with lanthanum, 1981 pp. 1.
- [20] A. Flórez, A. Herrera, M. Florez, *Phys. Status Solidi Curr. Top. Solid State Phys.* 4 (2007) 4156.
- [21] M.P. Hehlen, M.G. Brik, K.W. Krämer, *J. Lumin.* 136 (2013) 221.
- [22] B.J. Chen, L.F. Shen, E.Y.B. Pun, H. Lin, *Opt. Express* 20 (2012) 879.
- [23] Franziska Steudel, Marcel Dyrba, Stefan Schweizer, Fluorescent borate glass superstrates for high efficiency CdTe solar cells, in: R. Wehrspohn, A. Gombert (Eds.), Conference on Photonics for Solar Energy Systems IV Local: Brussels, Belgium, April 16–18, 2012, Photonics for Solar Energy Systems IV, Proceedings of SPIE, vol. 8438, 2012, Article:843803.
- [24] S. Kuhn, A. Herrmann, C. Rüssel, *J. Lumin.* 157 (2015) 390.
- [25] M. Seshadri, L.C. Barbosa, M. Radha, *J. Non. Cryst. Solids* 406 (2014) 62.
- [26] E.S. Yousef, *J. Alloy. Compd.* 561 (2013) 234.
- [27] A.S. Santos, N. Paola, D. Rojas, A. Herrera Influencia del ion samario trivalente en las propiedades térmicas de vidrios fluorinados, 1, 2009, pp. 419.
- [28] A. Rao, Y. Ahammed, R. Reddy, T.V. Rao, *Opt. Mater. (Amst.)* 10 (1998) 245.
- [29] K. Knoblochova, H. Ticha, J. Schwarz, L. Tichy, *Opt. Mater. (Amst.)* 31 (2009) 895.
- [30] A.E. Miller, K. Nassau, K.B. Lyons, M.E. Lines, *J. Non. Cryst. Solids* 99 (1988) 289.
- [31] H. Fan, G. Gao, G. Wang, L. Hu, *Solid State Sci.* 12 (2010) 541.
- [32] T. Seuthe, M. Grehn, A. Mermillod-Blondin, H.J. Eichler, J. Bonse, M. Eberstein, *Opt. Mater. Express* 3 (2013) 755.
- [33] N.F. Mott, E. a Davis, Electronic processes in non-crystalline materials, (1979).
- [34] Fouad El-Diasty, Fathy A. Abdel Wahab, Manal Abdel-Baki, Optical band gap studies on lithium aluminum silicate glasses doped with Cr^{3+} ions, *J. of Appl. Phys.* vol. 100 (Edição: 9, Número do 093511), (2006) 093511-1–093511-7.
- [35] M. Jayasimhadri, E.-J. Cho, K.-W. Jang, H.S. Lee, S. Il Kim, *J. Phys. D. Appl. Phys.* 41 (2008) 175101.
- [36] C.R. Kesavulu, C.K. Jayasankar, *J. Lumin.* 132 (2012) 2802.
- [37] Ş. Georgescu, A. Ştefan, A.-M. Voiculescu, O. Toma, *J. Lumin.* 162 (2015) 168.
- [38] O. Ravi, C. Madhukar Reddy, L. Manoj, B. Deva Prasad, *J. Mol. Struct.* 1029 (2012) 53.
- [39] P. Dorenbos, *J. Phys. Condens. Matter.* 15 (2003) 6249.
- [40] Y. Nageno, H. Takebe, K. Morinaga, T. Izumitani, *J. Non. Cryst. Solids* 169 (1994) 288.
- [41] A.A. Kaminskii, *Laser Crystals*, Springer, Berlin, 1981.
- [42] A. Kumar, D. Rai, S. Rai, *Spectrochim. Acta Part A Mol. Biomol. Spectrosc.* 59 (2003) 917.
- [43] P. Srivastava, S.B. Rai, D.K. Rai, *Spectrochim. Acta - Part A Mol. Biomol. Spectrosc.* 60 (2004) 637.
- [44] A.G. Souza Filho, J. Mendes Filho, F.E.A. Melo, M.C.C. Custódio, R. Lebullenger, A.C. Hernandez, *J. Phys. Chem. Solids* 61 (2000) 1535.
- [45] K. Annapurna, R.N. Dwivedi, A. Kumar, A.K. Chaudhuri, S. Buddhudu, *Spectrochim. Acta Part A Mol. Biomol. Spectrosc.* 56 (2000) 103.
- [46] P. Nachimuthu, R. Jagannathan, V. Nirmal Kumar, D. Narayana Rao, *J. Non. Cryst. Solids* 217 (1997) 215.
- [47] L. Boehm, R. Reisfeld, N. Spector, *J. Solid State Chem.* 28 (1979) 75.
- [48] R. Praveena, V. Venkatramu, P. Babu, C.K. Jayasankar, *Phys. B Condens. Matter* 403 (2008) 3527.
- [49] T. Suhasini, J. Suresh Kumar, T. Sasikala, K. Jang, H.S. Lee, M. Jayasimhadri, et al., *Opt. Mater. (Amst.)* 31 (2009) 1167.
- [50] L.F. Shen, B.J. Chen, E.Y.B. Pun, H. Lin, *J. Lumin.* 160 (2015) 138.
- [51] F. Fu, B. Chen, L. Shen, E.Y.B. Pun, H. Lin, *J. Alloy. Compd.* 582 (2014) 265.
- [52] R. Yu, Y. Guo, L. Wang, H.M. Noh, B.K. Moon, B.C. Choi, et al., *J. Lumin.* 155 (2014) 317.
- [53] I.I. Kindrat, B.V. Padyak, A. Drzewiecki, *J. Lumin.* 166 (2015) 264.